Catalysis Today 164 (2011) 23–27

Contents lists available at ScienceDirect

Catalysis Today

journal homepage: www.elsevier.com/locate/cattod

Hydrogen adsorption in metal organic frameworks by hydrogen spillover☆

Kuen-Song Lin*, Abhijit Krishna Adhikari, Kai-Che Chang, Mu-Ting Tu, Wei Lu

Department of Chemical Engineering and Materials Science/Fuel Cell Center, Yuan Ze University, 135, Yuan-Tung Rd., Chung-Li city 320, Tao-Yuan County, Taiwan, ROC

ARTICLE INFO

Article history:
Received 1 July 2010
Received in revised form 2 November 2010
Accepted 3 November 2010
Available online 10 December 2010

Keywords:
Metal organic framework
Bi-organic ligand
Spillover
Hydrogen adsorption
Fuel cell

ABSTRACT

A bi-organic-ligand type of $Zn_2(bdc)_2dabco$ MOFs was synthesized and characterized in the present work. The catalytic properties of Pt/AC and Pd/AC were studied for hydrogen spillover in $Zn_2(bdc)_2dabco$ modified by 5.0 wt.% of catalyst. The hydrogen adsorption capacity of modified $Zn_2(bdc)_2dabco$ was significantly enhanced up to 3.35 wt.% by using the secondary spillover with carbon bridges measured at 1.5 bar and 77 K. Moreover, the prepared MOFs were also identified using FE-SEM, HR-TEM, XRD, XANES/EXAFS, and BET N_2 adsorption isotherms techniques.

1. Introduction

The negative impact of greenhouse gases and the eventual depletion of fossil fuel reserves have increased the importance of developing alternative fuel sources that are strong, viable, and emission free. Hydrogen is considered a clean fuel that has a minimum impact on the environment nearly eliminating the levels of carbon dioxide and other greenhouse gas emissions. It is safe to manufacture, reliable and environmentally friendly [1]. However, developing safe, reliable, compact, and cost-effective H_2 storage technologies is one of the most technically challenging barriers to the widespread use of hydrogen as a form of energy as well as onboard vehicle application. Many efforts have been expended to finding efficient hydrogen storage materials to overcome this challenge. Concerning adsorbents, nanostructured carbon including activated carbon (AC) [2], carbon nanotubes [3] graphite nanofibers [4], zeolites [5] and complex metal hydrides [6] have been the major candidates for hydrogen storage. However, known carbon nanostructures and other studied materials cannot store a sufficient amount of H_2 required for transportation applications [7]. Metal-organic frameworks (MOFs) are a rapidly growing class of microporous materials that enable tailoring of regular porosity on a nanometer scale [8]. A variety of MOFs have been studied past few years for many potential applications, such as optics, sorptions depending on size and shape, catalysis, and most importantly gas storage [9]. Among the potential applications, particularly, MOFs have been explored as a viable H_2 storage material due to their relatively high hydrogen storage capacity and raised considerable interest in this field [10,11]. MOFs have the advantages of reversibility and fast kinetic ability in H_2 adsorption than complex metal hydrides. However, it is still far away from the hydrogen adsorption goal for onboard vehicle established by the United States Department of Energy (DOE).

The use of dissociation/spillover for H_2 storage, which is defined as the dissociative chemisorption of hydrogen on the metal and subsequent migration of atomic hydrogen onto the surface of the support such as AC, alumina and so on [12], is possible to increase the storage capacities in nanostructured materials such as MOFs. In the hydrogen spillover process, H_2 molecules dissociate into hydrogen atoms on the Pt or Pd catalyst (primary spillover source) supported by carbon materials such as AC. The dissociated atomic hydrogen migrates into carbon supports by primary spillover and finally into the MOFs through secondary spillover. Here, carbon support and MOFs act as primary and secondary spillover acceptor, respectively [13,14]. Recently, some groups have reported such improved H_2 storage in terms of secondary spillover mechanism [13–17]. Here we report, the synthesis method for the preparation of a hybrid composite of Pt/Pd-loaded AC–$Zn_2(bdc)_2dabco$ MOFs (bdc: 1,4-benzenedicarboxylic acid, dabco: 1,4-diazabicyclo[2.2.2]octane) that showed greatly enhanced hydrogen storage capacity by hydrogen spillover with carbon bridges. The parent materials such as $Zn_2(bdc)_2dabco$ and Pt or Pd loaded AC materials also characterized by field emission scanning electron microscopy (FE-SEM), high-resolution transmission electron microscopy (HR-TEM), X-ray diffraction (XRD), thermal

☆ Student Award Paper.

* Corresponding author. Tel.: +886 34638800x2574; fax: +886 34559373.
E-mail address: kslin@saturn.yzu.edu.tw (K.-S. Lin).

0920-5861/$ – see front matter © 2010 Elsevier B.V. All rights reserved.
doi:10.1016/j.cattod.2010.11.015

gravimetric analyzer (TGA), X-ray absorption near edge structure/extended X-ray absorption fine structure (XANES/EXAFS), and N_2 adsorptions analyses.

2. Experimental

2.1. Preparation of $Zn_2(bdc)_2dabco$

$Zn_2(bdc)_2dabco$ samples were prepared by heating a mixture of $Zn(NO_3)_2{\cdot}6H_2O$ (2.0 g, 6.72 mmol), H_2bdc (1.12 g, 6.73 mmol), and dabco (0.374 g, 3.34 mmol) suspended in dimethylformamide (DMF, 80 mL) in teflon-lined autoclave at 120 °C for 2 days. The colorless crystals formed were collected, washed several times with DMF and dried in reduced pressure at room temperature for one day and finally 80% yield was received. The detail experimental procedure of $Zn_2(bdc)_2dabco$ has been reported by Kim and coworkers [18] while we used the precursors twice in weight. All the chemicals (Sigma–Aldrich) were used without further purification.

2.2. Preparation of Pt or Pd-doped activated carbon (Pt/AC and Pd/AC)

In a typical procedure to synthesize the Pt or Pd-doped AC, 5.0 g of AC was immerged into 300 mL of 3 M nitric acid solution. The resulting mixture was heated to 60 °C and stirred for 1 h. After cooling to room temperature the AC was filtered and washed with water until the pH 5 had been reached and then dried in air. 0.5 g $PtCl_4$ or $PdCl_4$ was dissolved into another 300 mL of H_2O/ethylene glycol solution with the volume ratio of 1:2. Then the acid treated AC was added into the H_2O/ethylene glycol solution and stirred for 12 h at 110 °C. Then the resulted mixture was filtered and the solid residue was dried at 70 °C overnight in reduced pressure.

2.3. Preparation of Pt or Pd-doped AC–$Zn_2(bdc)_2dabco$

An effective bridged composite of Pt or Pd-doped AC–MOFs was done by building technique [14,19]. The catalyst containing 5 wt.% platinum or palladium supported on active carbon was used as the source for hydrogen dissociation. Carbon bridges between the source and receptor were formed by carbonization of sucrose that was previously introduced into a physical mixture with Pt or Pd/AC. The receptor/precursor/source ratio was fixed at 4:1:1 on the basis of the complete carbonization of the precursor. The resultant mixture was ground together for 1 h in ball mill and then subjected to the heating treatment procedures as described earlier [14].

2.4. Characterization of MOFs and composites

XRD measurements were conducted using standard powder diffraction procedures. The sample was smear-mounted onto a glass slide and then analyzed by Cu Kα radiation generated in a MAC Science, MXP18 diffractometer at 30 kV and 20 mA with a scan rate of $4^\circ(2\theta)$ min^{-1}. A diffraction experiment was run on standard glass slide for the background correction. The specific peak intensities and 2θ values recorded were further identified by a computer database system (JCPDS). FE-SEM (Hitachi, S-4700 Type II) and HR-TEM (Zeiss 10C) were performed to identify the morphologies, crystallinities, and particle size distribution. In case of FE-SEM scanning was performed on a sample powder previously dried and sputter coated with a thin layer of gold to avoid charging. Thermal decomposition was investigated using a TGA (model SDT 2960 & Thermal Analyst 2000, TA Instruments). Reaction temperatures and sample weights were recorded at 10 s intervals. About 30 mg of samples were heated from 298 to 973 K at a heating rate of 10 K min^{-1}. Nitrogen isotherms of the samples were measured at 77 K using an ASAP 2020 (Micromeritics). Prior to each measurement, samples were outgassed at 120 °C. Approximately 0.10 g of sample was used for these analyses. The surface area, S_{BET}, (Brunauer–Emmett–Teller method) [20] and the micropore volume, (Dubinin–Radushkevitch method) [21] were calculated from the isotherms.

XANES/EXAFS spectra were collected at the Wiggler beam line 17C1 at NSRRC, Taiwan. The electron storage ring were operated with energy of 1.5 GeV and a current of 100–200 mA. The double crystal monochromators employed at either beamline selected X-rays with energy resolving power ($E/\Delta E$) better than 7000, sufficient for most XAS measurements. Data were collected in fluorescence or transmission mode with a Lytle detector [22] for Zn (9662 eV) K edge at room temperature. The EXAFS function was derived from the raw absorption data through the pre-edge and post-edge background subtraction and then normalized with respect to the edge jump by using program package AUTOBK. After being k^3-weigted (k-range = 2.5–12.5 $Å^{-1}$), where k is the photoelectron wave number, the EXAFS function was Fourier transformed from k-space to r-space. Local structural parameters such as the bond distance R, coordination number N, and Debye–Waller factor σ, for different coordination shells surrounding the absorbing atoms were obtained through non-linear least-square fitting routine. All the computer programs were implemented in the software package UWXAFS 3.0. The phase shifts and backscattering amplitudes were theoretically calculated by using FEFF 8.20 code based on the crystallographic data of individual species [22,23].

2.5. Hydrogen adsorption measurement

Hydrogen isotherms were measured gravimetrically at 77 K using a method previously described by Eddaoudi et al. [24]. A Cahn Thermax 500 microgravimetric balance was used to measure the change in mass of samples suspended within a glass enclosure under a certain atmosphere which had a sensitivity of 1 μg. A pressure sensor, with a range of 0–68 atm (at 1000 °C) and sensitivity of 0.011 atm was used to measure the hydrogen pressure in the chamber. Samples were outgassed overnight in situ until constant mass was attained; these varied from 0.2 to 2.0 g. Prior to admittance of the analyte gas, the entire chamber and manifold were evacuated overnight. The system was purged at room temperature three times with the analyte gas before cooling to 77 K, and gases were passed through a molecular sieve trap immersed in liquid nitrogen to remove any condensable impurities or moisture before being

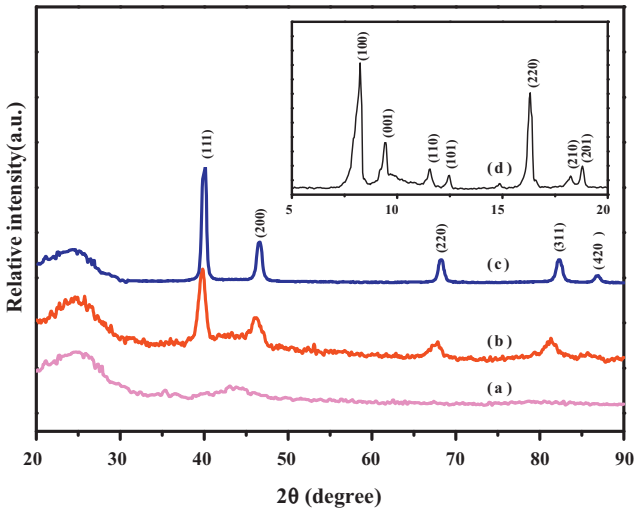

Fig. 1. XRD patterns of (a) acid-treated AC, (b) Pt-doped AC, (c) Pd-doped AC, and (d) synthesized $Zn_2(bdc)_2dabco$ MOFs (inset).

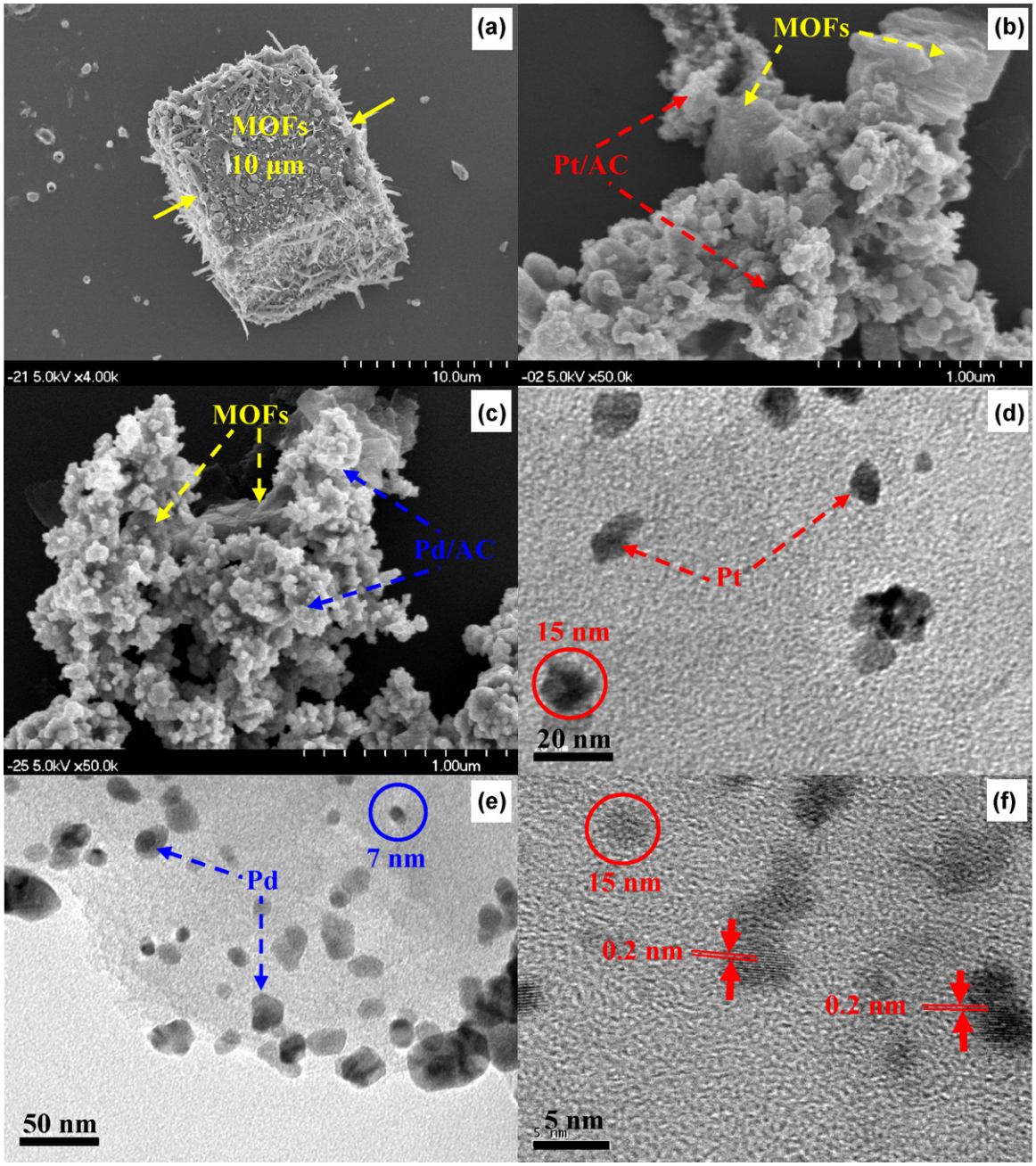

Fig. 2. FE-SEM images of the parent materials and composites (a) $Zn_2(bdc)_2dabco$ MOFs, (b) Pt-doped AC–$Zn_2(bdc)_2dabco$, (c) Pd-doped AC–$Zn_2(bdc)_2dabco$, HR-TEM images of (d) (f) Pt-doped AC and (e) Pd-doped AC.

exposed to the sample. The adsorbed amount of hydrogen gas was calculated after the buoyancy correction of the experiment. For the buoyancy correction, the volume of the sample container and the sample was determined using a helium measurement assuming that helium adsorption at room temperature can be neglected.

3. Results and discussion

The XRD patterns of the parent materials including acid treated AC are plotted in Fig. 1. All samples showed good crystallinity. The intensive peaks appearing at small 2θ angles in the XRD pattern of $Zn_2(bdc)_2dabco$ MOFs (inset of Fig. 1) are characteristics of porous materials which possess numerous pores or cavities. The diffraction peaks of our sample prepared in this study matched well with the already published XRD patterns on the same MOFs [18]. The XRD patterns of AC as well as Pt/AC and Pd/AC are shown in Fig. 1(a–c), respectively. These patterns show a broad and less intensive peak around $2\theta = 24^\circ$ can be attributed to the graphitic structure of AC. The other four peaks could be indexed to the (1 1 1), (2 0 0), (2 2 0), and (3 1 1) planes of Pt or Pd catalysts [25], respectively. The calculated mean particle size of the loaded Pt and Pd particles by Scherrer equation were about 14 and 18 nm, respectively. The particle size of synthesized $Zn_2(bdc)_2dabco$ sample was around 10–12 μm identified by FE-SEM micrographs shown in Fig. 2(a). After the bridge building treatment, Pt/AC or Pd/AC particles were well dispersed within the fine structure of MOFs and on the surface which acted as primary spillover source and receptor as shown in Fig. 2(b–c). The Pt and Pd particles were well dispersed in AC as shown in Fig. 2(d) and (e), respectively. The size range of Pt for 5 wt.% Pt/AC varied broadly from 5 to 45 nm as determined from extensive HR-

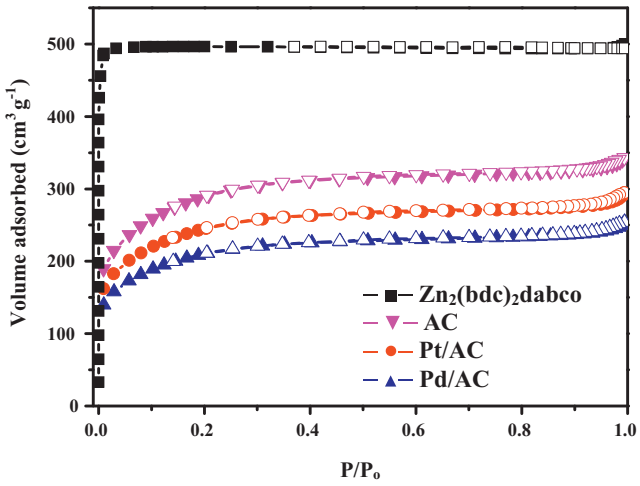

Fig. 3. Nitrogen isotherms at 77 K of $Zn_2(bdc)_2dabco$ MOFs, AC, Pt-doped AC, and Pd-doped AC. Filled and empty symbols represent the adsorption and desorption processes, respectively.

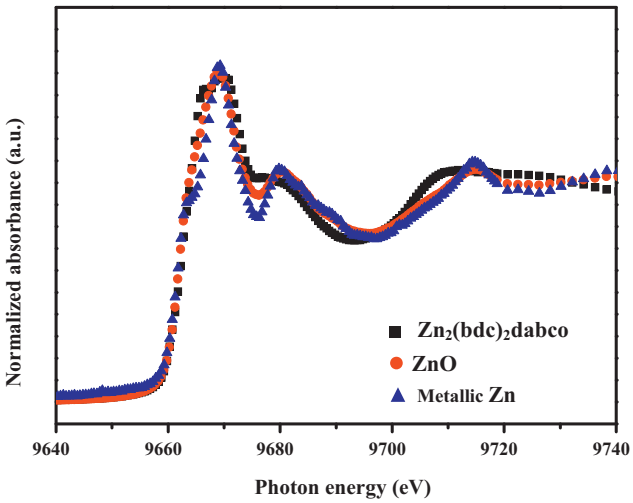

Fig. 4. Normalized Zn K-edge XANES spectra of $Zn_2(bdc)_2dabco$ MOFs, ZnO, and metallic Zn standards.

TEM examinations while the range was larger for Pd particles even around 80 nm. Formation of large Pt or Pd particles can be attributed to the aggregation of smaller particles. The dispersed particles in AC were well crystallized that facilitated the spillover of hydrogen by dissociating of hydrogen molecule into atomic hydrogen. From the close look of HR-TEM image of Pt/AC composite, it can be seen that the crystalline planes having diameter about 2 nm of Pt particle are randomly dispersed in AC (Fig. 2(f)).

Nonspecific physical adsorption of the $Zn_2(bdc)_2dabco$ and other composites was carried out to measure the total surface area and pore size distribution, as shown in Fig. 3. The BET surface areas and pore volumes of the materials measured by N_2 adsorption at 77 K are shown in Table 1. The specific surface area (SSA) of $Zn_2(bdc)_2dabco$ was 1433 $m^2\,g^{-1}$ with the pore volume of 0.769 $cm^3\,g^{-1}$. The BET SSA (or average pore diameters) of Pt/AC and Pd/AC were less (or larger) than that of the parent AC. The large loss of SSA and pore volume of AC after the Pt or Pd doping treatment can be attributed to the filling and blockage of micropores by the Pt or Pd particles distributed on the surface. Our synthesized $Zn_2(bdc)_2dabco$ MOFs showed excellent thermal stability carried out by TGA analysis. The weight loss during TGA analysis can be divided into three major sections. The first weight loss about 35% was observed around 100 °C. Evaporation of H_2O and the remaining solvent (DMF) caused this weight reduction. However, this result revealed that the MOFs absorb moisture from the air so easy. The second weight loss occurred within a wide range of temperature around 270–350 °C when unreacted BDC oxidized. After the oxidation of BDC, the organic linker of MOFs started to collapse slowly and finally the largest weight loss occurred around 452 °C which confirmed the total destruction of the frameworks. As the unreacted BDC lowers the surface area and blocks the pore of the framework it is important to remove it by washing or heat treatment.

The near edge region of the XANES spectrum is very informative on both the oxidation and coordination states of Zn species. The XANES spectra of synthesized MOFs with standard ZNO and Zn are shown in Fig. 4. The edge positions of standard Zn^{2+} and the central Zn metal of MOFs are 9661.79 and 9662.29, respectively. The offset is about 0.5 eV because of Zn ions are not entirely surrounded by oxygen atoms and form oxides (OH^-) with the covalent bond, thus it gives slight shift. However, the well-defined shoulders around 9661 eV are attributed to the 1s to $4p_{xy}$ transition that indicates the existence of Zn^{2+} species in MOFs. To obtain the information on local structure around metallic species in MOFs and other composites the EXAFS spectra have been analyzed. The obtained fine structural data form EXAFS spectra of $Zn_2(bdc)_2dabco$ MOFs, Pt/AC and Pd/AC are presented in Table 2. It can be seen that the MOFs have the Zn–O bond distance of 2.015 ± 0.02 Å with a coordination number of 3.42 ± 0.05. The Debye–Waller factors ($\Delta\sigma^2$) in all EXAFS data were less than 0.015 $Å^2$ which possess a good reliability of the obtained data.

Hydrogen can be stored via spillover in nanostructured materials. Secondary spillover is also possible to increase the H_2 storage capacity by using a catalyst that is capable of dissociating H_2. In this work, we used a catalyst containing 5 wt.% Pt/AC and Pd/AC as the source for H_2 dissociation. Here, active carbon was the primary receptor for hydrogen spillover. The catalyst and the $Zn_2(bdc)_2dabco$ (secondary spillover receptor) were introduced into a physical mixture. The hydrogen adsorption isotherm in Pt/AC–$Zn_2(bdc)_2dabco$ and Pd/AC–$Zn_2(bdc)_2dabco$ at 77 K are shown in Fig. 5. It can be seen that the H_2 adsorption on all samples showed a reversible Type I isotherm characteristic of a microporous material. Another feature was that for those samples, there was no apparent saturation value for the bridged samples up to 1.5 bar. This

Table 1
Determination of pore characteristics using nitrogen adsorption isotherms at 78 K of the MOFs and activated carbons porous materials.

Sample	Specific surface area[a] ($m^2\,g^{-1}$)	Pore volume[b] ($cm^3\,g^{-1}$)	Average pore diameter[c] (Å)
$Zn_2(bdc)_2dabco$	1433	0.769	21.32
AC	1108	0.552	22.76
Pt/AC	739	0.385	33.34
Pd/AC	882	0.443	36.81

[a] Specific surface areas were calculated by Brunauer–Emmett–Teller method.
[b] Pore volumes were calculated by Dubinin–Radushkevitch method.
[c] Average pore diameter was measured by BJH equation.

Table 2
Fine structural parameters of $Zn_2(bdc)_2dabco$ MOFs, Pt-doped AC, and Pd-doped AC analyzed from EXAFS.

Sample	Shell	CN[a](±0.05)	R[b] (±0.02)	$\Delta\sigma^{2c}$ ($Å^2$)
$Zn_2(bdc)_2dabco$	Zn–O	3.42	2.015	0.00342
Pt/AC	Pt–Pt	8.49	2.757	0.00586
Pd/AC	Pd–Pd	8.77	2.736	0.00622

[a] CN: coordination number.
[b] *R*: bond distance.
[c] σ: Debye–Waller factor.

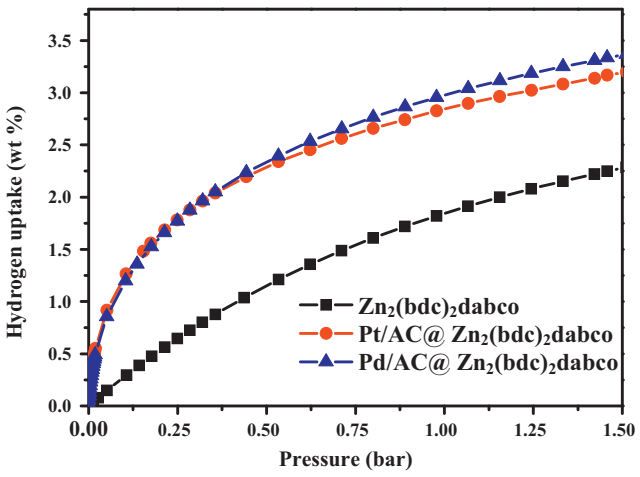

Fig. 5. Hydrogen adsorption isotherms of $Zn_2(bdc)_2dabco$ MOFs, Pt-doped AC–$Zn_2(bdc)_2dabco$, and Pd-doped AC–$Zn_2(bdc)_2dabco$ at $T = 77$ K and $P = 0$–1.5 bar.

result indicates that more hydrogen adsorption is possible at higher pressure. Park and coworkers [15] reported 1.89 wt.% of hydrogen adsorption on Pt loaded MOF-5 via spillover measured at 77 K and 1 bar pressure. Yang and coworker [14] reported the enhanced hydrogen adsorption on IRMOF-1 and IRMOF-8 via spillover. But the adsorption isotherms were measured at room temperature and 1 bar. The measured uptake of hydrogen was about 3.0 and 4.0 wt.% for bridged IRMOF-1 and IRMOF-8, respectively. Our obtained data are in good agreement with these previously reported data. Tsao and coworkers [16] explained the relation between lattice defects in the bridged samples and hydrogen adsorption via spillover on bridged IRMOF-8 sample. This result showed that the hydrogen adsorption on MOFs via spillover might depend on various structural parameters. Many authors have been observed that the hydrogen uptake at 77 K and elevated pressures correlates with the pore volume of the material. This can be easily described because at very high pressures the storage of hydrogen is mainly by condensation of H_2 molecules in the pores of the material. However, as hydrogen molecules are initially dissociated on metal nanoparticles and subsequently hydrogen atoms migrate on the surface of the receptor by spillover and diffusion, the adsorption by spillover is the interaction of hydrogen atoms with the surface sites of the material. Therefore, the pore volume of the material should not be the key factor in the net hydrogen storage capacity by spillover.

The mechanism proposed for the Pt or Pd/AC–$Zn_2(bdc)_2dabco$ can be summarized concisely: (1) adsorption of hydrogen molecule on the Pt or Pd surface, (2) dissociation of hydrogen molecule and chemisorption of atomic hydrogen on the surface, (3) migration of atomic hydrogen onto the AC support, and finally (4) chemisorptive spillover onto the $Zn_2(bdc)_2dabco$ MOFs. In addition, spillover is facilitated through the use of a carbon bridging compound between the Pt/AC or Pd/AC complex and the $Zn_2(bdc)_2dabco$ MOFs. As the atomic hydrogen adsorption is occurred not by condensation or adsorption of hydrogen molecules in case of spillover hydrogen adsorption, the surface adsorption sites of the material for hydrogen atoms adsorption should play an important role in determining the net storage capacity by spillover. A material with more and stronger surface adsorption sites for hydrogen atoms may adsorb more hydrogen via spillover. Some authors have found a linear correlation between the saturation H_2 uptake at 77 K and the surface area of MOFs [11,26]. However, this kind of linear correlation between the surface area and the adsorption capacity by bridged spillover was not observed in our study as well as reported by Yang and coworker [27]. Here we calculated the net hydrogen adsorption capacity via spillover by simple subtracting the amount adsorbed by physical adsorption ($Zn_2(bdc)_2dabco$ MOFs) from the total amount of hydrogen adsorbed by bridged Pt or Pd/AC–$Zn_2(bdc)_2dabco$ to determine the enhancing effect of spillover. The result showed that about 1.0–1.2 wt.% more hydrogen were adsorbed via spillover. This significant enhancement is clear evidence of the hydrogen spillover by carbon bridges and it indicated the creation of carbon bridges has remarkably importance for achieving higher hydrogen adsorption by secondary spillover.

4. Conclusions

The obtained results revealed that hydrogen storage by spillover is a promising technique to achieve higher hydrogen storage in MOFs. The highest measured H_2 uptake was 3.35 wt.% at 1.5 bar and 77 K by modifying the parent MOFs with 5 wt.% Pd loaded on AC. The secondary spillover technique by carbon bridges can be applied in other MOFs and higher sorption capacity can be expected. This result suggests that a further enhancement in hydrogen storage not only depends on the development of new MOFs materials, the modification of the MOFs with other materials can also lead to enhance the hydrogen adsorption.

References

[1] L.J. Murray, M. Dinc, J.R. Long, Chem. Soc. Rev. 38 (2009) 1294–1314.
[2] F.O. Erdogan, T. Kopac, Int. J. Hydrogen Energy 32 (2007) 3448–3456.
[3] E. Poirier, R. Chahine, T.K. Bose, Int. J. Hydrogen Energy 26 (2001) 831–835.
[4] A.D. Lueking, R.T. Yang, N.M. Rodriguez, R.T.K. Baker, Langmuir 20 (2004) 714–721.
[5] J.X. Dong, X.Y. Wang, H. Xu, Q. Zhao, J.P. Li, Int. J. Hydrogen Energy 32 (2007) 4998–5004.
[6] J. Wang, A.D. Ebner, J.A. Ritter, J. Phys. Chem. C 111 (2007) 14917–14924.
[7] A. Züttel, Mater. Today 6 (2003) 24–33.
[8] J.L.C. Rowsell, J. Eckart, O.M. Yaghi, J. Am. Chem. Soc. 127 (2005) 14904–14910.
[9] S. Kitagawa, R. Kitaura, S.-I. Noro, Angew. Chem., Int. Ed. 43 (2004) 2334–2375.
[10] D. Saha, Z. Wei, S. Deng, Int. J. Hydrogen Energy 33 (2008) 7479–7488.
[11] B. Panella, M. Hirscher, H. Pütter, U. Müller, Adv. Funct. Mater. 16 (2006) 520–524.
[12] S.T. Srinivas, P.K. Rao, J. Catal. 148 (1994) 470–477.
[13] Y. Li, R.T. Yang, J. Am. Chem. Soc. 128 (2006) 726–727.
[14] Y. Li, R.T. Yang, J. Am. Chem. Soc. 128 (2006) 8136–8137.
[15] S.J. Yang, J.H. Cho, K.S. Nahm, C.R. Park, Int. J. Hydrogen Energy 35 (2010) 13062–13067.
[16] C.-Y. Wang, C.-S. Tsao, M.-S. Yu, P.-Y. Liao, T.-Y. Chung, H.-C. Wu, M.A. Miller, Y.-R. Tzeng, J. Alloys Compd. 492 (2010) 88–94.
[17] C.-S. Tsao, M.-S. Yu, C.-Y. Wang, P.-Y. Liao, H.-L. Chen, U.-S. Jeng, Y.-R. Tzeng, H.-C. Wu, J. Am. Chem. Soc. 131 (2009) 1404–1406.
[18] D.N. Dybtsev, H. Chun, K. Kim, Angew. Chem., Int. Ed. 43 (2004) 5033–5036.
[19] A.J. Lachawiec, G.S. Qi, R.T. Yang, Langmuir 21 (2005) 11418–11424.
[20] S. Brunauer, P.H. Emmett, E. Teller, J. Am. Chem. Soc. 60 (1938) 309–319.
[21] M.M. Dubinin, in: P.L. Walker (Ed.), Chemistry and Physics of Carbon, vol. 2, Marcel Dekker, New York, 1966, pp. 51–120.
[22] F.W. Lytle, J. Synchrotron Rad. 6 (1999) 123–134.
[23] S.I. Zabinsky, J.J. Rehr, A. Ankudinov, M.J. Eller, Phys. Rev. B 52 (1995) 2995–3009.
[24] M. Eddaoudi, H.L. Li, O.M. Yaghi, J. Am. Chem. Soc. 122 (2000) 1391–1397.
[25] J.-M. Liu, H. Meng, J.-L. Li, S.-J. Liao, J.-H. Bu, Fuel Cells 7 (2007) 402–407.
[26] H. Frost, T. Duren, R.Q. Snurr, J. Phys. Chem. B 110 (2006) 9565–9570.
[27] Y. Li, R.T. Yang, AIChE J. 54 (2008) 269–279.